

Full-dimensional quantum mechanical study of  ${}^3\text{He} + {}^3\text{He} + X^- \rightarrow {}^3\text{He} + {}^3\text{He} X^-$  ( $X = \text{H}$  or  $\text{D}$ )Ming-Ming Zhao,<sup>1,\*</sup> Bin-Bin Wang<sup>2,\*</sup> and Yong-Chang Han<sup>1,3,†</sup><sup>1</sup>Department of Physics, Dalian University of Technology, Dalian 116024, China<sup>2</sup>Physics and Space Science College, China West Normal University, Nanchong 637002, China<sup>3</sup>DUT-BSU Joint Institute, Dalian University of Technology, Dalian 116024, China

(Received 3 September 2021; revised 14 November 2021; accepted 6 January 2022; published 13 January 2022)

The atom-atom-anion three-body recombination (TBR) of  ${}^3\text{He} + {}^3\text{He} + X^-$  ( $X = \text{H}$  or  $\text{D}$ ) systems at ultracold temperatures ( $T = 0.01 \sim 100$  mK) are studied by solving the Schrödinger equation in the adiabatic hyperspherical representation. It is found that for each system,  ${}^3\text{He} + {}^3\text{He} + \text{H}^-$  or  ${}^3\text{He} + {}^3\text{He} + \text{D}^-$ , the  $J^\Pi = 1^-$  symmetry dominates the TBR process, and the rates of TBR into  $l = 1$   ${}^3\text{He} X^-$  molecular anions are roughly three times as large as that into  $l = 0$   ${}^3\text{He} X^-$  molecular anions for  $T \in [0.01, 10]$  mK, where  $l$  denotes the two-body rotational quantum number. In addition, for a given product state, the TBR rates of the  ${}^3\text{He} + {}^3\text{He} + \text{H}^-$  system are larger than that of the  ${}^3\text{He} + {}^3\text{He} + \text{D}^-$  system by roughly two orders of magnitude which could be ascribed to the major nonadiabatic couplings between the entrance and recombination channels.

DOI: [10.1103/PhysRevResearch.4.013030](https://doi.org/10.1103/PhysRevResearch.4.013030)

## I. INTRODUCTION

Three-body recombination (TBR), as a typical scattering process, is one of the elemental types for chemical reactions. Generally, in a TBR process, three particles collide with each other, two particles form a molecule in a bound state, and the third particle takes away the binding energy. Compared with the two-body scattering process or bimolecular chemical reaction, TBR is usually of importance for cold or ultracold atoms and molecules of which the particles are considerably dense. Since part of the released binding energy is transformed into the kinetic energy of the third particle, TBR is a typical exothermic reaction. Thus, it is a major loss mechanism of Bose-Einstein condensation (BEC) [1–5]. This process may cause huge losses of the ultracold atomic gas and limits the density and lifetime of BEC [5,6]. Because the TBR process plays an important role in many physical processes, including trapping ultracold atoms [7,8], nuclear physics, the chemical dynamics of combustion and gas-phase system [4,9,10], etc., this process has attracted wide attention of many researchers.

When the three-body collision process involving charged particles, things become more different, and this has important implications for radiation physics [11,12]. It is the fundamental mechanism of the gaseous radiation detector, excimer lasers, and spectrometers [13,14]. Recently, the development of hybrid trap technology which combines neutral atom traps and ion traps, makes it possible to study the cold atom-ion interaction and the chemical reactions in mK regime [9,15–

21]. Most of the latest investigations of the atom-atom-ion TBR were concentrated on the state of the final products and the relationship between the collision energy and the TBR rate [9,20,22–25]. Pérez-Ríos and Greene have derived a classical energy scaling threshold law that the atom-atom-ion TBR rate  $K_3$  and the total collision energy  $E$  should follow the relationship of  $K_3 \propto E^{-3/4}$  [25]. In this classical threshold law, since the charge-induced dipole interaction  $C_4/r^4$  is more attractive than the van der Waals interaction  $C_6/r^6$ , it is considered that the TBR process for the atom-atom-ion systems are more obvious than that for the neutral atomic ternary systems and the molecular ion should dominate over the neutral molecule as the most formed product. This deduction has been confirmed experimentally for the TBR of  ${}^{87}\text{Ru} + {}^{87}\text{Ru} + {}^{138}\text{Ba}^+$  and  ${}^{87}\text{Ru} + {}^{87}\text{Ru} + {}^{87}\text{Ru}^+$  systems in the mK regime [9,20]. Although the study of TBR process of neutral-neutral-ion systems have some achievements in experiment, there are few theoretical investigations and still several issues to be investigated, for instance, the validity of the threshold law in the ultracold limit, i.e.,  $E \rightarrow 0$  [25]. Moreover, it is still difficult to perform quantum mechanical calculations of the TBR for the heavy systems such as  ${}^{87}\text{Ru} + {}^{87}\text{Ru} + {}^{138}\text{Ba}^+$ , because the number of atom-dimer and ion-dimer channels is very large. Therefore, the study for the TBR of neutral-neutral-ion systems is an emerging, developing research topic with many interesting aspects worth being studied [21,25,26].

In our previous works, the TBR processes of cold  ${}^4\text{He} + {}^4\text{He} + \text{H}^-/\text{D}^-$  and  ${}^4\text{He} + {}^4\text{He} + {}^6\text{Li}^-/{}^7\text{Li}^-$  systems were calculated by full-dimensional quantum mechanical treatment [22,27]. It was found that in the ultracold limit, the rate of TBR into  $l = 0$  molecular-anion products is larger than that into  $l = 1$  molecular-anion products for all these three-body systems. Moreover, for  ${}^4\text{He} + {}^4\text{He} + {}^6\text{Li}^-$  and  ${}^4\text{He} + {}^4\text{He} + {}^7\text{Li}^-$  systems, the rate of TBR into molecular-anion products is larger than that into the neutral molecular products, which is consistent with the classical prediction. However, for  ${}^4\text{He} + {}^4\text{He} + \text{H}^-$  and  ${}^4\text{He} + {}^4\text{He} + \text{D}^-$  systems,

\*These authors contributed equally to this work.

†Corresponding author: ychan@dlut.edu.cn

the rate of molecular-anion products after TBR process is roughly two orders of magnitude larger than that of neutral-molecule products, conversely, the rate of TBR into molecular-anion products is less than that into neutral-molecule products for the  ${}^4\text{He} + {}^4\text{He} + \text{D}^-$  system.

In this paper, we extend the investigation to another two systems,  ${}^3\text{He} + {}^3\text{He} + \text{X}^-$  ( $\text{X} = \text{H}$  or  $\text{D}$ ). Unlike the previous work containing two identical bosons, the present system contains two indistinguishable fermions, which is the simplest system containing two fermions where the TBR process can occur. This provides a theoretical basis for future research on more complex systems. Through the full-dimensional quantum mechanical calculations, we have studied the distribution of final products after the TBR process in the ultracold limit and the dependence of the TBR rate on the collision energy for different partial waves. We expect to understand the mechanism for the different behavior by substituting fermions for bosons in this work.

The paper is organized as follows. In Sec II, we explain the treatments of the atom-atom-ion three-body recombination and give all necessary formulas for theoretical calculation. In Sec III, the results are shown and discussed in detail. A conclusion is given in Sec IV. Atomic units are used throughout except when explicitly stated otherwise.

## II. THEORETICAL APPROACH

The TBR rate of the three-body systems can be obtained by solving the Schrödinger equation using the adiabatic hyperspherical representation [28,29] and  $R$ -matrix method [30,31]. After the separation of the center-of-mass motion, any three-particle systems can be described by six coordinates. We solve the Schrödinger equation for three interacting particles in an improved Smith-Whiten hyperspherical coordinates  $\{R, \Omega\} \equiv \{R, \theta, \phi, \alpha, \beta, \gamma\}$ .  $R$  is the hyperradius, the only length parameter, defining the overall size of this system, and  $\theta$  and  $\phi$  are hyperangles, which are utilized to describe the internal motion of the three-body system. The remaining three are taken to be Euler angles, which are used to describe the orientation of the body-fixed frame relative to the space-fixed frame. A schematic figure of the definitions of the Euler angles ( $\alpha, \beta, \gamma$ ) and the axes of the body-fixed frame used in the calculations is shown in Fig. 1.

In these hyperspherical coordinates, we rewrite the Schrödinger equation with a rescaled wave function which is related to  $\Psi(R, \Omega)$  in the usual Schrödinger equation by  $\psi(R, \Omega) = R^{5/2}\Psi(R, \Omega)$ . The Schrödinger equation for a three-body system interacting through the potential  $V(R, \theta, \phi)$  reads [32,33]

$$\left[ -\frac{1}{2\mu} \frac{\partial^2}{\partial R^2} + \frac{\Lambda^2 + \frac{15}{4}}{2\mu R^2} + V(R, \theta, \phi) \right] \psi(R, \Omega) = E \psi(R, \Omega), \quad (1)$$

where  $\Lambda^2$  is the squared ‘‘grand angular momentum operator’’ [32,34].  $\mu$  is the three-body reduced mass and is given as

$$\mu = \sqrt{\frac{m_1 m_2 m_3}{m_1 + m_2 + m_3}}, \quad (2)$$

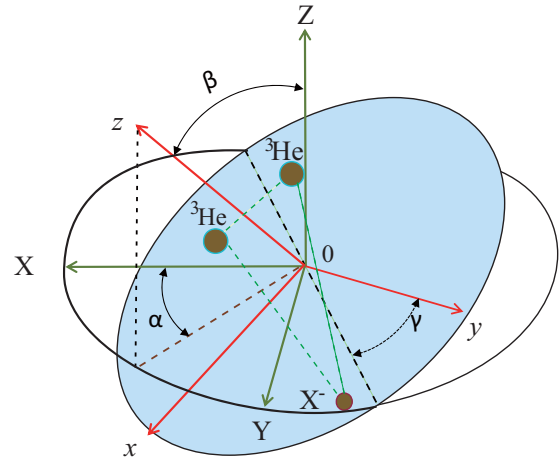


FIG. 1. Euler angles ( $\alpha, \beta, \gamma$ ) relating the space-fixed frame  $XYZ$  and the body-fixed frame  $xyz$ . The green solid lines represent the axes of the space-fixed frame and the red solid lines represent the axes body-fixed frame. The three particles lie in the body-fixed frame, and the center of mass of the three particles is crossed by the  $z$  axis.

where  $m_i$  ( $i = 1, 2, 3$ ) is the mass of particle  $i$ , with  $i = 1$  assigned as the hydrogen anion, i.e.,  $\text{H}^-$  or  $\text{D}^-$ , and  $i = 2$  and  $3$  as the two indistinguishable fermionic helium atoms.

The potential energy  $V(R, \theta, \phi)$  is approximately to be a sum of the three pairwise two-body potentials [30]

$$V(R, \theta, \phi) = V_{\text{HeH}}(r_{12}) + V_{\text{HeHe}}(r_{23}) + V_{\text{HeH}}(r_{31}), \quad (3)$$

where  $r_{ij}$  is the internuclear distance between given two particles, and in terms of the hyperspherical coordinates, it can be expressed as [22,29]

$$r_{12} = 2^{-1/2} d_{12} R [1 + \sin \theta \cos(\phi + \phi_{12})]^{1/2}, \quad (4)$$

$$r_{23} = 2^{-1/2} d_{23} R (1 + \sin \theta \cos \phi)^{1/2}, \quad (5)$$

$$r_{31} = 2^{-1/2} d_{31} R [1 + \sin \theta \cos(\phi - \phi_{31})]^{1/2}, \quad (6)$$

with  $\phi_{12} = 2 \tan^{-1}(m_2/\mu)$ ,  $\phi_{31} = 2 \tan^{-1}(m_3/\mu)$ . The ranges of the hyperangles are taken as  $\theta \in [0, \pi/2]$  and  $\phi \in [0, \pi]$ .  $d_{ij}$  are defined as

$$d_{ij} = \sqrt{\frac{m_k(m_i + m_j)}{\mu(m_i + m_j + m_k)}}, \quad (7)$$

where the indices ( $i, j, k$ ) are a cyclic permutation of (1, 2, 3).

For the He-He dimer potential  $V_{\text{HeHe}}(r)$ , we adopt the representation designed by Jeziorska *et al.* [35]. For the He- $\text{H}^-$  potential  $V_{\text{HeH}^-}(r)$ , the potential of Casalegno *et al.* is adopted [36]. These potentials have been successfully applied to the calculations of several three-body collisions [27,29,37,38], and both  $V_{\text{HeHe}}(r)$  and  $V_{\text{HeH}^-}(r)$  are fitted with analytical models to the precise *ab initio* computed points at small distance, while the asymptotic part of the He-He interaction potential is established by taking the precise Van der Waals constants from  $C_6$  to  $C_{16}$ , and that of He- $\text{H}^-$  interaction is determined by the  $C_4$  which is the accurate coefficient of the anion-induced dipole interaction. For  ${}^3\text{He}-\text{H}^-$  and  ${}^3\text{He}-\text{D}^-$  interaction, there

TABLE I. Two-body rovibrational energies  $E_{\nu l}$ , with  $\nu$  the vibrational quantum number and  $l$  the rotational quantum number, and  $s$ -wave scattering lengths calculated using the dimer potentials from Refs. [36,38].

System	$(\nu, l)$	$E_{\nu l}(\text{a.u.})$	$E_{\nu l}(\text{mK} \times k_B)$	$a(\text{a.u.})$	$a(\text{\AA})$
${}^3\text{HeH}^-$	(0,0)	$-1.63 \times 10^{-6}$	-514.79	5.52	2.92
	(0,1)	$-4.77 \times 10^{-8}$	-15.08		
${}^3\text{HeD}^-$	(0,0)	$-3.12 \times 10^{-6}$	-985.11	-65.01	-34.4
	(0,1)	$-1.66 \times 10^{-6}$	-524.01		

are two bound states, i.e.,  $(\nu = 0, l = 0)$  and  $(\nu = 0, l = 1)$ , where  $\nu$  and  $l$  denote the vibrational and rotational quantum numbers. Whereas, for  ${}^3\text{He}-{}^3\text{He}$  interaction, there is no bound state. Here, for convenience, the collective vibrational quantum number  $\nu$  used for these molecular anions will be removed in the following discussion. The bound state energies and corresponding  $s$ -wave scattering lengths calculated by these two interaction potentials are shown in Table I. Note that an absolutely accurate potential energy surface should include the retardation and nonadditive three-body terms, whereas no nonadditive three-body potential is available in the literature for the  $\text{He} + \text{He} + \text{H}^-$  system. Thus, we solely use the sum of the relevant pairwise potentials. In addition, the hyperfine interactions among these three particles are also neglected in this work. Taking the hyperfine interactions into

account would include more channels and require computational powers beyond the state-of-the-art. Here, due to the close structures of the helium atoms and the hydrogen anion in the electronically ground states, the hyperfine interactions only include interactions associated with nuclear spins, which generally tend to be very weak compared with the electronic potentials. How much such interactions influence the TBR process is an intriguing scientific issue and requires much further study in the future.

In our calculations, in order to solve Eq. (1), the first step is to solve the fixed- $R$  adiabatic eigenvalue equation for a given symmetry  $J^\Pi$ , where the  $J$  and  $\Pi$  are the total nuclear orbital momentum and parity, and obtain the adiabatic eigenfunctions  $\Phi_v^{J^\Pi}(R; \Omega)$  and the eigenvalues  $U_v(R)$

$$\left[ \frac{\Lambda^2}{2\mu R^2} + \frac{15}{8\mu R^2} + V \right] \Phi_v^{J^\Pi}(R; \Omega) = U_v(R) \Phi_v^{J^\Pi}(R; \Omega). \quad (8)$$

Then, the wave function  $\psi(R, \Omega)$  can be expanded on the complete orthonormal set of adiabatic eigenfunctions, i.e., angular wave functions or channels,  $\Phi_v^{J^\Pi}(R; \Omega)$ ,

$$\psi(R, \Omega) = \sum_{v=1}^N F_v(R) \Phi_v^{J^\Pi}(R; \Omega), \quad (9)$$

where the quantum number  $v$  distinguishes different channels and  $N$  is the number of total channels we adopted.

Insertion of Eq. (9) into Eq. (1) leads to a set of one-dimensional coupled differential equations

$$\left[ -\frac{1}{2\mu} \frac{d^2}{dR^2} + W_v(R) \right] F_v(R) - \frac{1}{2\mu} \sum_{v' \neq v} \left[ 2P_{vv'}(R) \frac{d}{dR} + Q_{vv'}(R) \right] F_{v'}(R) = E F_v(R), \quad (10)$$

where  $W_v(R)$  is effective potential,  $P_{vv'}(R)$  and  $Q_{vv'}(R)$  are nonadiabatic couplings, respectively. The explicit forms of these three terms are defined as follows:

$$W_v(R) = U_v(R) - \frac{Q_{vv}(R)}{2\mu}, \quad (11)$$

$$P_{vv'}(R) = \left\langle \Phi_v^{J^\Pi}(R; \Omega) \left| \frac{\partial}{\partial R} \right| \Phi_{v'}^{J^\Pi}(R; \Omega) \right\rangle_\Omega, \quad (12)$$

$$Q_{vv'}(R) = \left\langle \Phi_v^{J^\Pi}(R; \Omega) \left| \frac{\partial^2}{\partial R^2} \right| \Phi_{v'}^{J^\Pi}(R; \Omega) \right\rangle_\Omega. \quad (13)$$

The subscript  $\Omega$  of the bracket signifies that integrals are carried out only over the angular coordinates  $\Omega$ .

From the definition of  $P_{vv'}(R)$  and Eq. (10), it can be seen that  $P_{vv'}(R)$  is an important term and is generally adopted to define the nonadiabatic coupling strength  $f_{vv'}(R)$ , which is used to characterize the magnitude of nonadiabatic coupling between two channels [39]

$$f_{vv'}(R) = \frac{|P_{vv'}(R)|^2}{2\mu |U_{v'}(R) - U_v(R)|}. \quad (14)$$

In order to solve Eq. (8), we expand the channel function on Wigner  $D$  functions

$$\Phi_v^{J^\Pi}(R; \Omega) = \sum_K \varphi_{Kv}^{J^\Pi}(R; \theta, \phi) D_{KM}^J(\alpha, \beta, \gamma), \quad (15)$$

where the quantum numbers  $K$  and  $M$  represent the projection of  $J$  onto the body-fixed and space-fixed  $z$  axes, respectively.  $K = J, J-2, \dots, -(J-2), -J$  for the ‘‘parity-favored’’ case, i.e.,  $\Pi = (-1)^J$ , and  $K = J-1, J-3, \dots, -(J-3), -(J-1)$  for the ‘‘parity-unfavored’’ case,  $\Pi = (-1)^{J+1}$ , where  $K$  should be even for even parity and odd for odd parity. The resulting complex coupled equations in  $\theta$  and  $\phi$  are solved by expanding  $\varphi_{Kv}^{J^\Pi}(R; \theta, \phi)$  onto a direct product of fifth-order basis splines [40]. The identical particle symmetry of two  ${}^3\text{He}$  particles can be built into the adiabatic equations via the boundary conditions [38]. At  $\phi = 0$ ,

$$\begin{aligned} &(-1)^{J+K} \varphi_{-Kv}^{J^\Pi}(R; \theta, 0) - \varphi_{Kv}^{J^\Pi}(R; \theta, 0), \\ &(-1)^{J+K+1} \frac{\partial \varphi_{-Kv}^{J^\Pi}}{\partial \phi} \Big|_{\phi=0} = -\frac{\partial \varphi_{Kv}^{J^\Pi}}{\partial \phi} \Big|_{\phi=0}, \end{aligned} \quad (16)$$

and at  $\phi = \pi$ ,

$$\begin{aligned} &(-1)^J \varphi_{-Kv}^{J^\Pi}(R; \theta, \pi) = -\varphi_{Kv}^{J^\Pi}(R; \theta, \pi), \\ &(-1)^{J+1} \frac{\partial \varphi_{-Kv}^{J^\Pi}}{\partial \phi} \Big|_{\phi=\pi} = -\frac{\partial \varphi_{Kv}^{J^\Pi}}{\partial \phi} \Big|_{\phi=\pi}, \end{aligned} \quad (17)$$

therefore we only need to consider the range  $\phi \in [0, \pi]$ .

In order to calculate accurately the adiabatic potential  $U_v(R)$  and channel function  $\Phi_v^{J^\Pi}(R; \Omega)$  in Eq. (8), the mesh points in  $\theta$  and  $\phi$  should be designed carefully as described

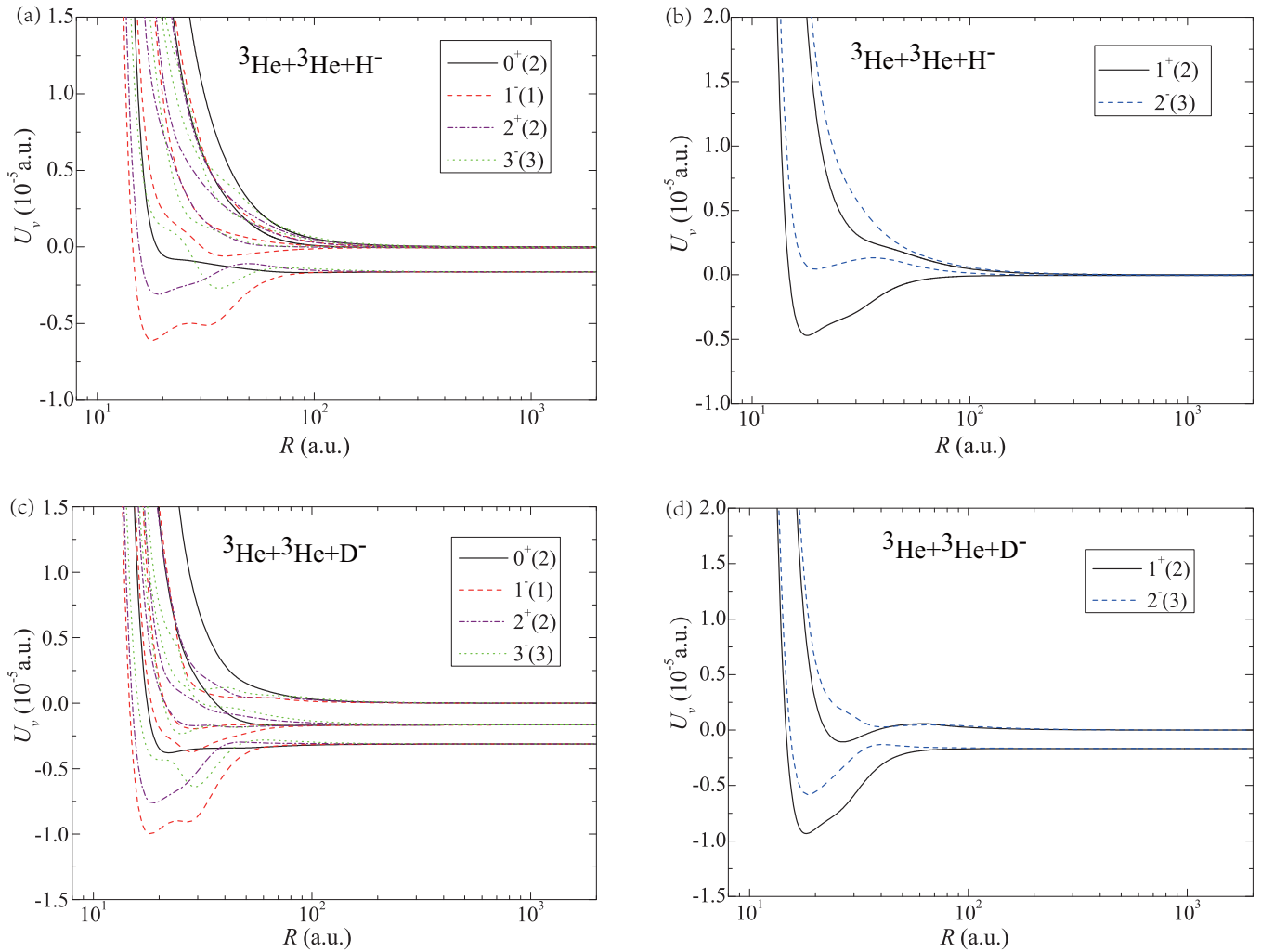


FIG. 2. The adiabatic potential curves  $U_v(R)$  of the  ${}^3\text{He} + {}^3\text{He} + \text{H}^-$  and  ${}^3\text{He} + {}^3\text{He} + \text{D}^-$  systems contains all recombination channels and the lowest entrance channel. (a) and (c) are the parity-favored cases for the two systems, i.e.,  $J^\Pi(\lambda_{\min})=0^+(2)$ ,  $1^-(1)$ ,  $2^+(2)$ ,  $3^-(3)$  symmetries. (b) and (d) are the parity-unfavored cases for the two system, i.e.,  $J^\Pi(\lambda_{\min})=1^+(2)$ ,  $2^-(3)$  symmetries. The  $\lambda_{\min}$  represents the minimum  $\lambda$  in the view of the symmetry for the two  ${}^3\text{He}$  atoms.

in Ref. [38]. In practice, we generate the basis splines for  $\theta$  from 100 mesh points, while we use 180 mesh points for  $\phi$ . Thereafter, we could solve  $\Phi_v^{J^\Pi}(R; \Omega)$  and obtain  $U_v(R)$  which is converged to at least six digits for all the channels calculated from  $R = 2$  a.u. to 2000 a.u. In order to track the abrupt changes in the nonadiabatic couplings, a hyperradial grid with approximately 2000 mesh points is used in this range, and for  $R > 2000$  a.u., the adiabatic potentials and nonadiabatic couplings are extrapolated [31,41]. The  $\Phi_v^{J^\Pi}(R; \Omega)$  is *a priori* complex quantities which may have arbitrary phases upon numerical diagonalization. Making  $P_{vv'}(R)$  and  $Q_{vv'}(R)$  continuous in  $R$  is important for solving Eq. (10), thus a consistent phase convention is required [42].

We solve the coupled one-dimensional equation Eq. (10) using the adiabatic finite element method [31,39]. In this work, about  $1.2 \times 10^4$  finite element sectors are adopted and distributed as  $R_i \propto i^3$  from  $R = 2$  to 2000 a.u., and 14 adiabatic channels are used. For  $R > 2000$  a.u., for each de Broglie wavelength, the density of finite element sectors is fixed to eight element sectors. Then we extract the  $S$  matrix

by matching the numerical solutions. Finally, the total recombination rate  $K_3$  is expressed as [43]

$$K_3 = \sum_{J,\Pi} K_3^{J^\Pi} = 2! \sum_{J,\Pi} \sum_i \frac{32(2J+1)\pi^2}{\mu k^4} |S_{f \leftarrow i}^{J,\Pi}|^2, \quad (18)$$

where  $K_3^{J^\Pi}$  is the partial recombination rate corresponding to  $J^\Pi$  symmetry,  $i$  and  $f$  label the incident and recombination channels respectively, and  $k = \sqrt{2\mu E}$  is the hyperradial wave number in the incident channels.  $S_{f \leftarrow i}^{J,\Pi}$  is the scattering matrix element from the channel  $i$  to the channel  $f$ .

### III. RESULTS AND DISCUSSIONS

Since the  ${}^3\text{He} - X^-$  ( $X=\text{H}$  or  $\text{D}$ ) dimer has two bound states ( $l = 0$  and  $l = 1$ ), the TBR processes of  ${}^3\text{He} + {}^3\text{He} + X^-$  systems include both the parity-favored and parity-unfavored cases. The corresponding adiabatic potential curves  $U_v(R)$  as function of the hyperradius  $R$  for the groups of the parity-favored and parity-unfavored cases are shown in Figs. 2(a)

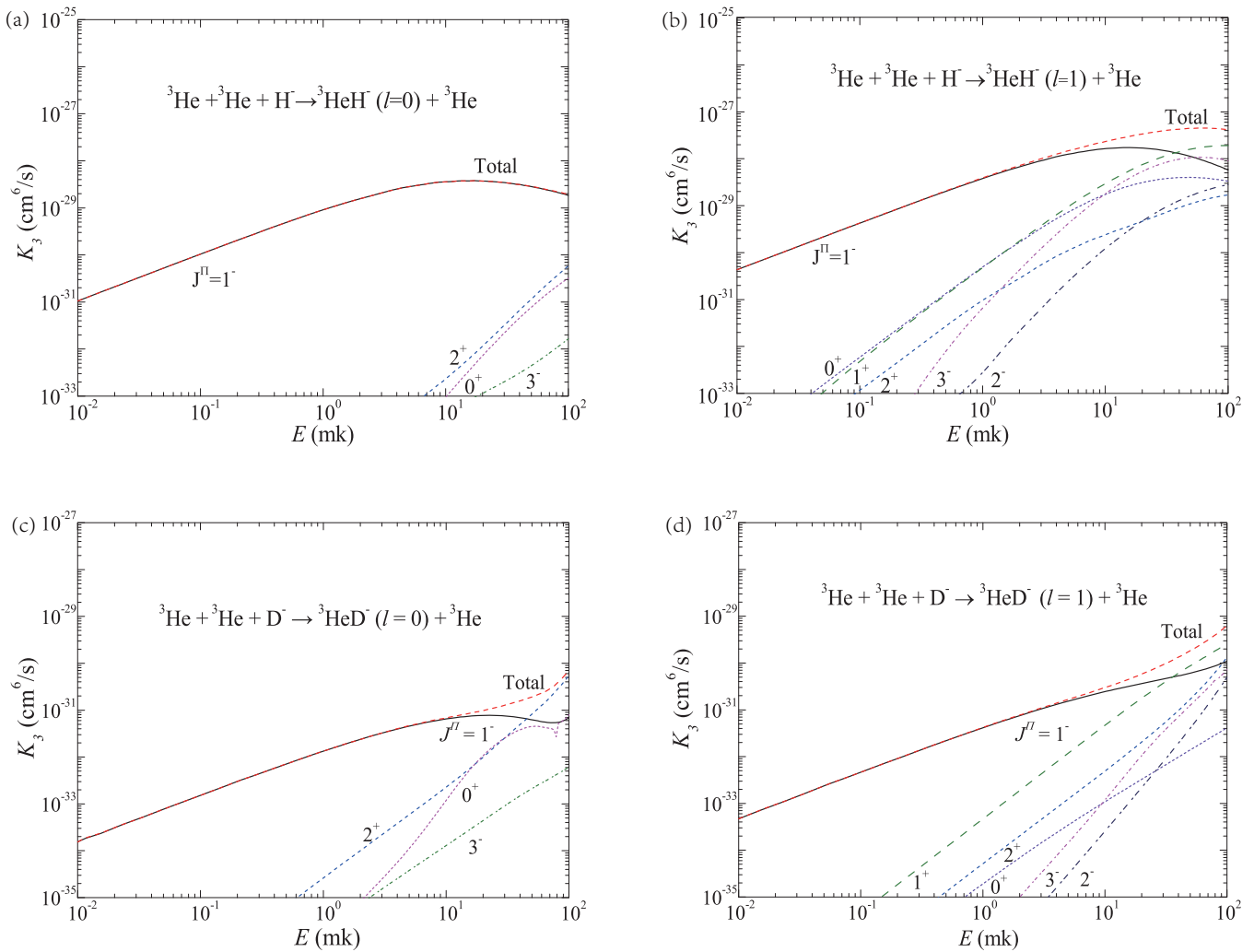


FIG. 3. Total and partial atom-atom-anion three-body recombination rates as function of collision energy, for the  ${}^3\text{He} + {}^3\text{He} + \text{H}^-$  [(a) and (b)] and  ${}^3\text{He} + {}^3\text{He} + \text{D}^-$  systems [(c) and (d)].

and 2(b) for the  ${}^3\text{He} + {}^3\text{He} + \text{H}^-$  system, and for comparison, those for the  ${}^3\text{He} + {}^3\text{He} + \text{D}^-$  system are shown in Figs. 2(c) and 2(d). Taking the  ${}^3\text{He} + {}^3\text{He} + \text{H}^-$  system for example, for each parity case, the curves represent the lowest entrance channel (three free particles) and all recombination channels (a dimer and a free particle). The total angular momentum  $J$  of the system is set to be less than 4. For each  $J^\Pi$  symmetry,  $U_v(R)$  changes dramatically and displays sharp nonadiabatic avoided crossings in the short  $R$  range. For the parity-favored case, as shown in Fig. 2(a), the lowest two curves of  $U_v(R)$  for  $3^-$  symmetry illustrate a sharp nonadiabatic avoided crossing at  $R \approx 20$  a.u., and for the parity-unfavored case, the adiabatic potentials of  $2^-$  symmetry in Fig. 2(b) show a sharp nonadiabatic avoided crossing at  $R \approx 30$  a.u.. Actually, as we will discuss later, it is more convenient to understand the characteristics of the nonadiabatic couplings by using the definition of  $f_{vv'}(R)$  in Eq. (14). By comparing Figs. 2(c) and 2(d) with Figs. 2(a) and 2(b), a strong differences between the two systems can be revealed in the adiabatic potentials. Instead of comparing the difference between the two systems in the adiabatic potentials for each  $J^\Pi$  symmetry, we would like to compare the TBR rates of the two systems and find

the most important  $J^\Pi$  symmetry for TBR process. Then, we present a detailed comparison between the two systems for the given  $J^\Pi$  symmetry which dominates the TBR process.

The TBR rates  $K_3$  for both parity-favored and parity-unfavored cases ( $J < 4$ ) associated with both the  ${}^3\text{He} + {}^3\text{He} + \text{H}^-$  and  ${}^3\text{He} + {}^3\text{He} + \text{D}^-$  systems are calculated and are shown in Fig. 3. We have checked that the partial TBR rates for the  $J \geq 4$  cases have negligible contribution to the total TBR rate for both the two systems in the considered collision energy range. It is also worth noticing that the partial TBR rate for  $J^\Pi = 3^+$  symmetry which contributes to the formation of  $l = 1$   ${}^3\text{HeX}^-$  molecular anions is vanishingly small, due to its relatively large  $\lambda_{\min}$  which is the minimum value of  $\lambda$  allowed by the permutation symmetry for the two  ${}^3\text{He}$  atoms. Here,  $\lambda(\lambda + 4)$  is the eigenvalues of  $\Lambda^2$  [27]. Thus, we do not show the partial TBR rate of  $J^\Pi = 3^+$ . As can be seen from Fig. 3,  $K_3$  is mainly contributed by only few partial waves, especially for  $E < 10$  mK. At even lower collision energies ( $E < 1$  mK), the red dashed curve denoting the total  $K_3$  is almost on top of the black solid one which denotes the contribution of the partial wave  $J^\Pi = 1^-$ . This indicates that the  $J^\Pi = 1^-$  partial wave dominates the TBR process for the

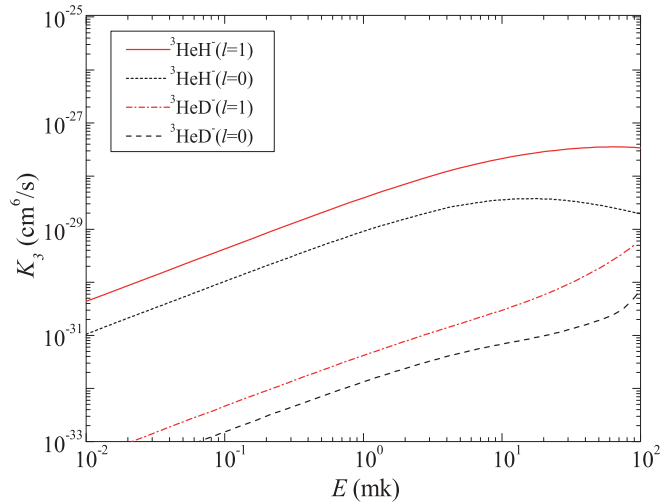


FIG. 4. Comparison of the total three-body recombination rates leading to different molecular-anion products for  ${}^3\text{He} + {}^3\text{He} + \text{H}^-$  and  ${}^3\text{He} + {}^3\text{He} + \text{D}^-$  systems.

two systems in this energy range. The partial TBR rates for the two systems behave roughly as  $K_3^{J^\Pi} \propto E^{\lambda_{\min}}$ , i.e., roughly follow the prediction of the generalized Winger's threshold law [7]. Thus,  $K_3$  is suppressed by decreasing the collision energy  $E$ . This is entirely different from our previous calculations on the TBRs of the  ${}^4\text{He} + {}^4\text{He} + X^-$  ( $X = \text{H}, \text{D}, {}^6\text{Li}, {}^7\text{Li}$ ) systems, in which  $K_3$  always approaches to a certain constant for  $E \rightarrow 0$  [22,27]. This can be ascribed to the substitution of the two identical fermions  ${}^3\text{He}$  for the bosons  ${}^4\text{He}$ .

The contributions from the higher partial waves can be distinguishable with the increase of the collision energy. The rates of recombination to the  $l = 0$   ${}^3\text{He}X^-$  molecular anions for the two systems are shown in Figs. 3(a) and 3(c), respectively. Although the partial TBR rates for  $J^\Pi = 0^+, 2^+$ , and  $3^-$  symmetries for the two systems increase with  $E$ , their contributions to total TBR rate of  ${}^3\text{He} + {}^3\text{He} + X^-$  are still negligible. On the contrary, the contributions from the partial TBR rates for  $J^\Pi = 0^+$  and  $2^+$  to  $l = 1$   ${}^3\text{HeD}^-$  are distinguishable for  $E > 10$  mK, as shown in Fig. 3(d). For  $E > 40$  mK, the partial TBR rate for  $J^\Pi = 2^+$  is even greater than that for  $J^\Pi = 1^-$ . The TBR rates relevant to the formation of  $l = 1$   ${}^3\text{He}X^-$  molecular anions are shown in Figs. 3(b) and 3(d). The  $J^\Pi = 0^+, 1^+$  and  $2^+$  symmetries have the same  $\lambda_{\min} = 2$ , and according to the generalized Winger's threshold law mentioned above, their partial TBR rates have similar behaviors with the variation of  $E^2$  [7]. The same statements can be applied to the  $J^\Pi = 3^-$  and  $2^-$  symmetries for which  $\lambda_{\min} = 3$ . For  $E > 30$  mK, the partial TBR rate for  $J^\Pi = 1^-$  does not dominate the total TBR any more.

For a more visual representation, we show the total TBR rate  $K_3$  as function of the collision energies  $E$  for the two systems in Fig. 4. It can be seen that the TBR rates of the  ${}^3\text{He} + {}^3\text{He} + \text{H}^-$  system are always larger than that of the  ${}^3\text{He} + {}^3\text{He} + \text{D}^-$  system. The rates of TBR into  ${}^3\text{HeH}^-$  ( $l = 0$  and  $l = 1$ ) molecular anions are roughly two orders of magnitude larger than that of TBR into  ${}^3\text{HeD}^-$  ( $l = 0$  and  $l = 1$ ) molecular anions, within the considered collision energy range. Additionally, for given collision system, the TBR rate

for the  $l = 1$  molecular anions is always greater than that for the  $l = 0$  ones. It is worth noting that for  $E > 10$  mK, the rates of TBR into  ${}^3\text{HeD}^-$  molecular anion increase drastically, while that into  $l = 0$   ${}^3\text{HeH}^-$  molecular anions does not present such a strong increase rate, furthermore the rate of TBR into  $l = 1$   ${}^3\text{HeH}^-$  molecular anions even decreases. This is consistent with the variations of the TBR rates of the partial waves that we have discussed above in Fig. 3. Although in this low collision energy range, the total TBR rates for  ${}^3\text{HeD}^-$  ( $l = 0$  and  $l = 1$ ) molecular anions are lower than that for  ${}^3\text{HeH}^-$  ( $l = 0$  and  $l = 1$ ) molecular anions, it can be expected that the former can be comparable with the latter for higher collision energy.

The above differences between the TBR rates  $K_3$  of the two systems, can be understood by considering the behavior of the adiabatic potentials  $U_v(R)$  and the corresponding nonadiabatic couplings  $f_{vv'}(R)$ . Since the partial TBR rate for  $J^\Pi = 1^-$  dominates the total TBR in most of the considered collision energy range, we focus on the recombination of this symmetry. In this symmetry, we consider interactions among the lowest entrance channel and all the three recombination channels. The three recombination channels, are labeled as  $v = 1$  for  ${}^3\text{He}X^-$  ( $l = 0$ ) +  ${}^3\text{He}$  and  $v = 2, 3$  for  ${}^3\text{He}X^-$  ( $l = 1$ ) +  ${}^3\text{He}$ . The lowest entrance channel is label as  $v = 4$  for the three-particle continuum state.

We first consider the  ${}^3\text{He} + {}^3\text{He} + \text{H}^-$  system. Figure 5(a) shows the lowest four adiabatic potentials corresponding to the above four channels and the nonadiabatic coupling strengths  $f_{vv'}(R)$  between each two channels. As shown in Fig. 5(a),  $f_{23}(R)$  is the most strong nonadiabatic coupling out of the six couplings. This is because the two channels ( $v = 2$  and  $3$ ) are close in energy. The energy asymptotes of the two channels coincide, i.e., the bound energy of  $l = 1$   ${}^3\text{HeH}^-$  molecular anions. Thus,  $f_{23}(R)$  does not directly affect the TBR rate for  $l = 1$   ${}^3\text{HeH}^-$  molecular anions though it is great in amplitude. Obviously, the interactions between the entrance channel  $v = 4$  and the recombination channels  $v = 1, 2, 3$  can directly affect the TBR rate. Although  $f_{4,v}(R)$  is very large in the relatively short hyperradial range of  $R < 100$  a.u., the major pathways [44] associated with direct transitions from the lowest incident channel to the recombination channels tend to be difficult to occur in this short  $R$  range. It is because in this short  $R$  range, the adiabatic potential energy corresponding to the lowest incident channel is several orders of magnitude larger than the collision energy considered in the present work, cf. Fig. 5(a). Thus, the nonadiabatic couplings between the lowest incident channel and the recombination channels for  $R < 100$  a.u. have little effect on the total TBR rates, and the transitions from the lowest incident channel to the recombination channels mainly occur in the large  $R$  range. Nevertheless, it is still worth noticing that once any recombination channel has been populated, the population will then be redistributed among all these relevant recombination channels due to their nonadiabatic couplings. Here, the couplings between recombination channels in the short  $R$  range will affect the population redistribution process, because the recombination channels are energetically accessible in this region.

For clarity, the TBR process can be described as "jumps" of flow [27]. The TBR process can be consider to be a flow of the population from the entrance channel to the recombina-

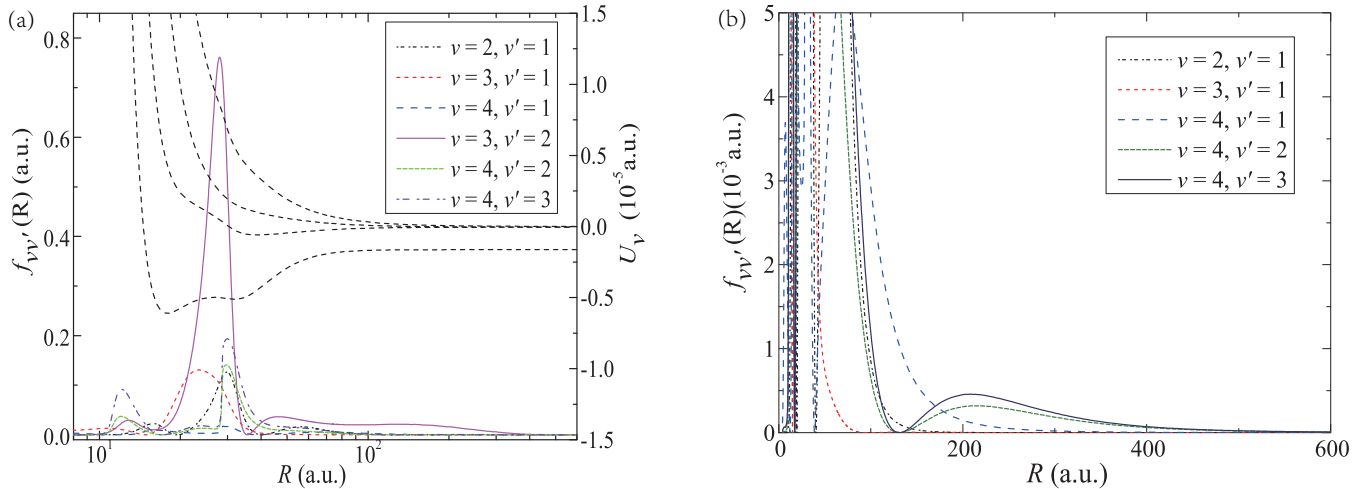


FIG. 5. For the  $J^\pi=1^-$  symmetry of  ${}^3\text{He} + {}^3\text{He} + \text{H}^-$  system: (a) the lowest four adiabatic potential curves  $U_v$  (black dashed curves), corresponding to three recombination channels and one entrance channel and their nonadiabatic coupling strength  $f_{vv'}(R)$  (color curves); (b) the major nonadiabatic coupling strengths responsible for the three-body recombination process.

tion channel. On one hand, from the point view of potential energy, there are two recombination channels ( $v = 2, 3$ ) to the formation of  $l = 1$   ${}^3\text{HeH}^-$  molecular anions, while the number of recombination channels to  $l = 0$   ${}^3\text{HeH}^-$  molecular anions is only one ( $v = 1$ ). Additionally, the potential energies for channels  $v = 2, 3$  are both higher than that for channel  $v = 1$ , and the former two are closer to the entrance channel  $v = 4$  than the latter one. As a result, we can expect that the TBR rate  $K_3$  for  $l = 1$   ${}^3\text{HeH}^-$  molecular anions should be larger than that for  $l = 0$   ${}^3\text{HeH}^-$  molecular anions. On the other hand, from the point of view of the interactions between the entrance channel and the recombination channels, we can also deduce the same expectation as above. As shown in Fig. 5(b),  $f_{42}(R)$  and  $f_{43}(R)$  present relatively strong couplings in a widespread  $R$  region from roughly 100 to 500 a.u., and these two couplings can be considered to be two major wide passages connecting with the entrance channel ( $v = 4$ ) and the recombination channels ( $v = 2, 3$ ), resulting in the formation of the  $l = 1$   $\text{HeH}^-$  molecular anions. However, for formation of the  $l = 0$   $\text{HeH}^-$  molecular anions, the incident flow has to “jump” into channel  $v = 1$  from channel  $v = 4$  via the nonadiabatic coupling  $f_{41}(R)$  which locates in a relatively smaller  $R$  region (from roughly 100 to 300 a.u.). Thus, in the large  $R$  region where the transition from the lowest incident channel to the recombination channels mainly occurs, the TBR rate for  $l = 1$   $\text{HeH}^-$  molecular anions is expected to be greater than that for  $l = 0$   $\text{HeH}^-$  molecular anions. In addition, although  $f_{41}(R)$  is greater than  $f_{42}(R)$  and  $f_{43}(R)$  in the short  $R$  region from roughly 100 to 170 a.u.,  $f_{21}(R)$  shows considerable coupling strength which constructs a pathway for  ${}^3\text{HeH}^-$  transferring from  $l = 0$  back to  $l = 1$ . This loss mechanism further suppresses the TBR rate leading to formation of  $l = 0$   $\text{HeH}^-$  molecular anions. In brief, by taking the  ${}^3\text{He} + {}^3\text{He} + \text{H}^-$  system for example, based on the properties of  $U_v(R)$  and  $f_{vv'}(R)$ , we can deduce that the TBR rate for  $l = 1$  is greater than that for  $l = 0$ , which is consistent with the calculation results in Fig. 4. One can perform the similar deduction procedure in the other system, and draw the same conclusion.

Hereafter, we focus on the difference between the two systems in the two aspects of  $U_v(R)$  and  $f_{vv'}(R)$ . Figure 6(a) shows the adiabatic potentials corresponding to the lowest entrance channel and all recombination channels for the  ${}^3\text{He} + {}^3\text{He} + \text{D}^-$  (dashed curves) and  ${}^3\text{He} + {}^3\text{He} + \text{H}^-$  (solid curves) systems. Due to the heavier mass of the D atom, the adiabatic potentials for the  ${}^3\text{He} + {}^3\text{He} + \text{D}^-$  system show stronger attraction in short  $R$  range, while the energy difference between the asymptotes of the entrance and each recombination channels is relatively larger, compared to those for the other system. In the hyperspherical coordinates, a large energy difference between the adiabatic potentials generally corresponds to a smaller nonadiabatic coupling strength, cf. Eq. (14). Thus, the TBR process tends to be difficult to occur when the energy difference between the asymptotes of the lowest incident and highest recombination channels is relatively large. So, it may be relatively harder for the TBR to occur in the  ${}^3\text{He} + {}^3\text{He} + \text{D}^-$  system than the other system. Particularly, due to the larger energy difference between the asymptotes of the entrance and each recombination channels for the  ${}^3\text{He} + {}^3\text{He} + \text{D}^-$  system, its nonadiabatic coupling in the long  $R$  range is weaker than that for the other system. Figure 6(b) shows the contrast of the major nonadiabatic coupling strengths for the two systems. It can be seen that the strong nonadiabatic couplings of the  ${}^3\text{He} + {}^3\text{He} + \text{D}^-$  system mainly take place in the short  $R$  range ( $R < 100$  a.u.), where the TBR process can be difficult to occur. The nonadiabatic couplings for the  ${}^3\text{He} + {}^3\text{He} + \text{D}^-$  system are weaker than those for the  ${}^3\text{He} + {}^3\text{He} + \text{H}^-$  system in the large  $R$  range ( $R \geq 100$  a.u.), which is consistent with the above discussions based on potentials. Thus, the rate for the formation of the  ${}^3\text{HeD}^-$  molecular anions is much less than that of  ${}^3\text{HeH}^-$  molecular anions.

#### IV. CONCLUSION

In this work, the three-body recombination process of the  ${}^3\text{He} + {}^3\text{He} + \text{X}^-$  systems has been investigated using the

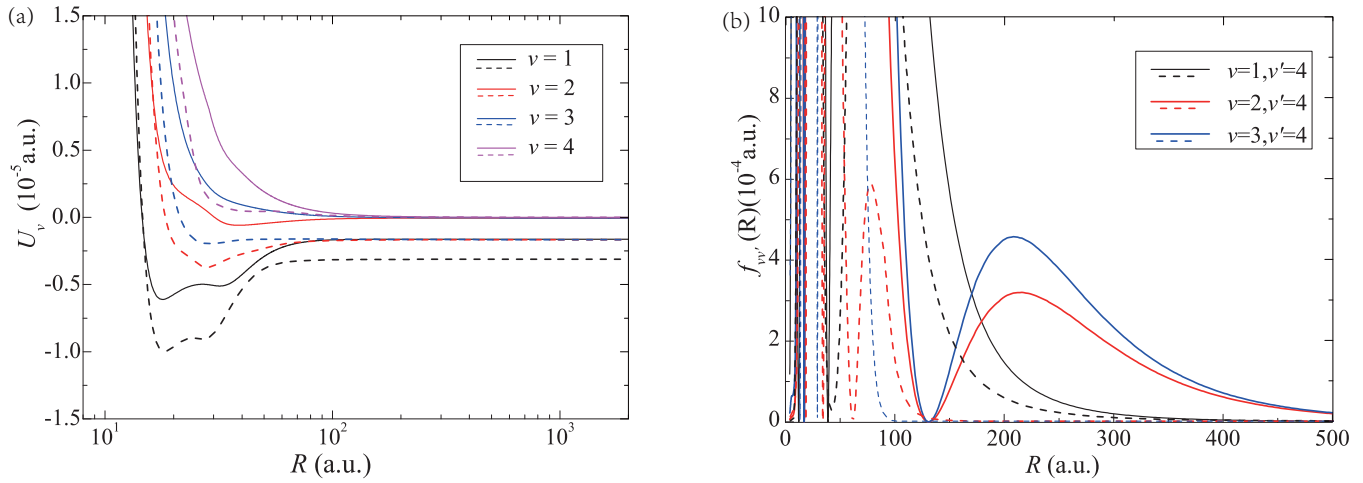


FIG. 6. (a) The lowest entrance channel and all recombination channels for the  ${}^3\text{He} + {}^3\text{He} + \text{H}^-$  system (solid curves) and  ${}^3\text{He} + {}^3\text{He} + \text{D}^-$  system (dashed curves) for  $J^\Pi = 1^-$  symmetry; (b) A comparison of the corresponding major nonadiabatic coupling strengths.

adiabatic hyperspherical recombination. It is found that the TBR process is dominated by only few partial waves, especially to the formation of  $l = 1$   ${}^3\text{HeH}^-$  molecular anions. The TBR process is dominated by the  $J^\Pi = 1^-$  symmetry. The rates of TBR into  $l = 1$   ${}^3\text{He}X^-$  molecular anions are larger than that into  $l = 0$   ${}^3\text{He}X^-$  molecular anions and the total rate of the  ${}^3\text{He} + {}^3\text{He} + \text{H}^-$  system is always larger than the  ${}^3\text{He} + {}^3\text{He} + \text{D}^-$  system in our considered energy region. This is ascribed to the major nonadiabatic couplings among the entrance and recombination channels.

#### ACKNOWLEDGMENTS

The project was supported by the National Key R&D Program of China No. 2018YFA0306503; the National Natural Science Foundation of China under Grants No. 21873016, No. 22103063, and No. 12174044; the Fundamental Research Funds of China West Normal University Grant No. 412775; International Cooperation Fund Project of DBJI No. ICR2105; the Fundamental Research Funds for the Central Universities (DUT21LK08).

- [1] H. F. Hess, D. A. Bell, G. P. Kochanski, D. Kleppner, and T. J. Greytak, Temperature and Magnetic Field Dependence of Three-Body Recombination in Spin-Polarized Hydrogen, *Phys. Rev. Lett.* **52**, 1520 (1984).
- [2] J. Stenger, S. Inouye, M. R. Andrews, H. J. Miesner, D. M. Stamper-Kurn, and W. Ketterle, Strongly Enhanced Inelastic Collisions in a Bose-Einstein Condensate near Feshbach Resonances, *Phys. Rev. Lett.* **82**, 2422 (1999).
- [3] B. D. Esry, C. H. Green, and J. P. Burke, Recombination of Three Atoms in the Ultracold Limit, *Phys. Rev. Lett.* **83**, 1751 (1999).
- [4] T. Weber, J. Herbig, M. Mark, H. C. Nägerl, and R. Grimm, Three-Body Recombination at Large Scattering Lengths in an Ultracold Atomic Gas, *Phys. Rev. Lett.* **91**, 123201 (2003).
- [5] C. Chin, R. Grimm, P. Julienne, and E. Tiesinga, Feshbach resonances in ultracold gases, *Rev. Mod. Phys.* **82**, 1225 (2010).
- [6] E. A. Burt, R. W. Ghrist, C. J. Myatt, M. J. Holland, E. A. Cornell, and C. E. Wieman, Production of Two Overlapping Bose-Einstein Condensates by Sympathetic Cooling, *Phys. Rev. Lett.* **78**, 586 (1997).
- [7] B. D. Esry, C. H. Greene, and H. Suno, Threshold laws for three-body recombination, *Phys. Rev. A* **65**, 010705(R) (2001).
- [8] R. Wynar, R. S. Freeland, D. J. Han, C. Ryu, and D. J. Heinzen, Molecules in a Bose-Einstein condensate, *Science* **287**, 1016 (2000).
- [9] A. Krüchow, A. Mohammadi, A. Härter, J. H. Denschlag, J. Pérez-Ríos, and C. H. Greene, Energy Scaling of Cold Atom-Ion Three-Body Recombination, *Phys. Rev. Lett.* **116**, 193201 (2016).
- [10] C. A. Stan, M. W. Zwierlein, C. H. Schunck, S. M. F. Raupach, and W. Ketterle, Observation of Feshbach Resonances between Two Different Atomic Species, *Phys. Rev. Lett.* **93**, 143001 (2004).
- [11] P. N. B. Neves, C. A. N. Conde, and L. M. N. Távora, A new experimental technique for positive ion drift velocity measurements in noble gases: Results for xenon ions in xenon, *Nucl. Instrum. Methods Phys. Res., Sect. A* **580**, 66 (2007).
- [12] P. N. B. Neves, C. A. N. Conde, and L. M. N. Távora, The  $X^+ + 2X \rightarrow X_2^+ + X$  reaction rate constant for Ar, Kr and Xe, at 300 K, *Nucl. Instrum. Methods Phys. Res., Sect. A* **619**, 75 (2010).
- [13] J. D. C. Jones, D. G. Lister, D. P. Wareing, and J. Twiddy, The temperature dependence of the three-body reaction rate coefficient for some rare-gas atomic ion-atom reactions in the range 100-300K, *J. Phys. B* **13**, 3247 (1980).
- [14] V. O. Papanyan, G. T. Nersisyan, S. A. Ter-Avetisyan, and F. K. Tittle, Vacuum ultraviolet afterglow emission of rare gases and their mixtures, *J. Phys. B* **28**, 807 (1995).
- [15] C. Zipkes, S. Palzer, C. Sias, and M. Köhl, A trapped single ion inside a Bose-Einstein condensate, *Nature (London)* **464**, 388 (2010).

- [16] S. Schmid, A. Härter, and J. H. Denschlag, Dynamics of a Cold Trapped Ion in a Bose-Einstein Condensate, *Phys. Rev. Lett.* **105**, 133202 (2010).
- [17] F. H. J. Hall, M. Aymar, N. Boulouta-Maata, O. Dulieu, and S. Willitsch, Light-Assisted Ion-Neutral Reactive Processes in the Cold Regime: Radiative Molecule Formation versus Charge Exchange, *Phys. Rev. Lett.* **107**, 243202 (2011).
- [18] K. Ravi, S. Lee, A. Sharma, G. Wreth, and S. A. Rangwala, Cooling and stabilization by collisions in a mixed ion-atom system, *Nat. Commun.* **3**, 1126 (2012).
- [19] F. H. J. Hall and S. Willitsch, Millikelvin Reactive Collisions between Sympathetically Cooled Molecular Ions and Laser-Cooled Atoms in an Ion-Atom Hybrid Trap, *Phys. Rev. Lett.* **109**, 233202 (2012).
- [20] A. Härter, A. Krüchow, A. Brunner, W. Schnitzler, S. Schmid, and J. H. Denschlag, Single Ion as a Three-Body Reaction Center in an Ultracold Atomic Gas, *Phys. Rev. Lett.* **109**, 123201 (2012).
- [21] A. Krüchow, A. Mohammadi, A. Härter, and J. H. Denschlag, Reactive two-body and three-body collisions of  $\text{Ba}^+$  in an ultracold Rb gas, *Phys. Rev. A* **94**, 030701(R) (2016).
- [22] B. B. Wang, S. H. Jing, and T. X. Zeng, Cold atom-atom-anion three-body recombination of  $^4\text{He}^4\text{He}^x\text{Li}^-$  ( $x = 6$  or  $7$ ) systems, *J. Chem. Phys.* **150**, 094301 (2019).
- [23] B. B. Wang, Scattering length scaling rules for atom-atom-anion three-body recombination of zero-energy  $^4\text{He}^4\text{He}^6\text{Li}^-$  system, *Phys. Chem. Chem. Phys.* **23**, 14617 (2021).
- [24] J. Pérez-Ríos, S. Ragole, J. Wang, and C. H. Greene, Comparison of classical and quantal calculations of helium three-body recombination, *J. Chem. Phys.* **140**, 044307 (2014).
- [25] J. Pérez-Ríos and C. H. Greene, Communication: Classical threshold law for ion-neutral-neutral three-body recombination, *J. Chem. Phys.* **143**, 041105 (2015).
- [26] A. Härter and J. H. Denschlag, Cold atom-ion experiments in hybrid traps, *Contemp. Phys.* **55**, 33 (2014).
- [27] B. B. Wang, Y. C. Han, W. Gao, and S. L. Cong, Cold atom-atom-ion three-body recombination of  $^4\text{He}^4\text{He}X^-$  ( $X = \text{H}$  or  $\text{D}$ ), *Phys. Chem. Chem. Phys.* **19**, 22926 (2017).
- [28] B. R. Johnson, On hyperspherical coordinates and mapping the internal configurations of a three body system, *J. Chem. Phys.* **73**, 5051 (1980).
- [29] H. Suno and B. D. Esry, Adiabatic hyperspherical study of triatomic helium systems, *Phys. Rev. A* **78**, 062701 (2008).
- [30] M. Aymar, C. H. Greene, and E. Luc-Koenig, Multichannel Rydberg spectroscopy of complex atoms, *Rev. Mod. Phys.* **68**, 1015 (1996).
- [31] J. P. Burke, Jr., Theoretical investigation of cold alkali atom collisions, Ph.D. thesis, University of Colorado, 1999.
- [32] B. K. Kendrick, R. T. Pack, R. B. Walker, and E. F. Hayes, Hyperspherical surface functions for nonzero total angular momentum. I. Eckart singularities, *J. Chem. Phys.* **110**, 6673 (1999).
- [33] B. R. Johnson, The quantum dynamics of three particles in hyperspherical coordinates, *J. Chem. Phys.* **79**, 1916 (1983).
- [34] B. Lepetit, Z. Peng, and A. Kuppermann, Calculation of bound rovibrational states on the first electronically excited state of the  $\text{H}_3$  system, *Chem. Phys. Lett.* **166**, 572 (1990).
- [35] M. Jeziorska, W. Cencek, K. Patkowski, B. Jeziorski, and K. Szalewicz, Pair potential for helium from symmetry-adapted perturbation theory calculations and from supermolecular data, *J. Chem. Phys.* **127**, 124303 (2007).
- [36] M. Casalegno, M. Mella, G. Morosi, and D. Bressanini, Quantum Monte Carlo study of the  $\text{H}^-$  impurity in small helium clusters, *J. Chem. Phys.* **112**, 69 (2000).
- [37] H. Suno and B. D. Esry, Adiabatic hyperspherical study of weakly bound helium-helium-alkali-metal triatomic systems, *Phys. Rev. A* **82**, 062521 (2010).
- [38] H. Suno and B. D. Esry, Three-body recombination in cold helium-helium-alkali-metal-atom collisions, *Phys. Rev. A* **80**, 062702 (2009).
- [39] H. Suno and B. D. Esry, C. H. Greene, and J. P. Burke, Three-body recombination of cold helium atoms, *Phys. Rev. A* **65**, 042725 (2002).
- [40] C. de Boor, *A Practical Guide to Splines* (Springer, New York, 1978).
- [41] E. Nielsen, D. V. Fedorov, A. S. Jensen, and E. Garrido, The three-body problem with short-range interactions, *Phys. Rep.* **347**, 373 (2001).
- [42] B. B. Wang, Y. C. Han, and S. L. Cong, Role of sharp avoided crossings in short hyper-radial range in recombination of the cold  $^4\text{He}_3$  system, *J. Chem. Phys.* **145**, 204304 (2016).
- [43] Y. Wang, J. P. D’Incao, and B. D. Esry, Cold three-body collisions in hydrogen-hydrogen-alkali-metal atomic systems, *Phys. Rev. A* **83**, 032703 (2011).
- [44] J. P. D’Incao and B. D. Esry, Scattering Length Scaling Laws for Ultracold Three-Body Collisions, *Phys. Rev. Lett.* **94**, 213201 (2005).